# Towards a multiphase finite element code for the evaluation of volcanic risk

Andrea Montanino[1], Alessandro Franci[2], Giulio Zuccaro[1]

[1] *Department of Structures for engineering and Architecture (DiST) University of Naples "Federico II" - Naples - ITALY*
*{andrea.montanino, zuccaro}@unina.it*

[2] *International Centre for Numerical Methods in Engineering Universitat Politècnica de Catalunya - Barcelona - SPAIN*
*falessndro@cimne.upc.edu*

**Abstract.** The evaluation of volcanic risk is of great relevance for the institutions of Civil Protection, which are required to design emergency plans and to take all the necessary countermeasures against this type of catastrophic natural hazard. The assessment of volcanic risk can be performed basing on the observation and statistical interpretation of historical data, or using numerical instruments for the analysis of possible scenarios. In this work, we focus on the latter strategy and develop a novel Finite Element formulation for the description of multiphase flows, with the final aim of simulating pyroclastic density currents at the scale of urban settlements. Pyroclastic flows are here modeled numerically by solving the conservation laws of mass, linear momentum, and energy, under the hypotheses of kinetic and thermal equilibrium. In order to avoid unphysical oscillations of solution variables, the Finite Element formulation is stabilized with a recent implementation of the Variational Multiscale method for multiphase flows. Benchmark problems in the field of compressible monophase and multiphase flows are here analyzed to prove accuracy and robustness of the proposed formulation. A realistic scale case of pyroclastic gravity current hitting some buildings is also presented. The test shows the potential of the proposed approach to evaluate quantities of interest for the evaluation of the hazard deriving from volcanic events, such as the generated pressure on civil constructions.

**Keywords:** Volcanic risk assessment, multiphase flows, Variational Multiscale method

## 1. Introduction

The evaluation of the volcanic risk is of primary importance for the departments of Civil Protection, since on these predictions are based the design of the emergency plans (Baxter et al., 2005) and mitigation strategies (Zuccaro and De Gregorio, 2019), including the systems of building protection, such as panels and resistant fixtures (Zuccaro and Leone, 2012; Iacuaniello et al., 2020).

For the evaluation of the volcanic risk, it is crucial to have an estimation of those quantities that could be dangerous for urban settlements, such as the pressure on buildings and the temperature of the pyroclastic flow. This could be done basing on observations, historical reports (Zuccaro et al., 2008), and/or numerical simulations (Neri et al., 2003; Esposti Ongaro et al., 2007).

The aim of this work is to propose a reliable numerical model for the prediction of the effect of this natural hazard on civil constructions. In particular, the objective is to evaluate the pressure and temperature fields acting on civil buildings for different geometrical characteristics of the urban settlements and intensities of the volcanic eruption event.

The pyroclastic flow is here modeled by solving the *mixture* equations of conservation of the mass, linear momentum, and energy, following the formulation proposed by Pelanti and LeVeque (2006) and developed for the case of thermal and kinetic equilibrium by Cerminara et al. (2016). Such formulation holds at a distance from the volcano source that depends on the characteristics of the pyroclastic flow.

The resultant system of equations has the same nature as that of monophase compressible flows. It is well-known (Bochev et al., 2004; Tezduyar and Sathe, 2003) that the Eulerian Finite Element methods suffer from numerical instability when applied to advection-diffusion problems with a dominant convective term. For this reason, the numerical method needs to be stabilized. Among different stabilizing tools proposed in the literature, here we adopt the Variational Multiscale Method (Hughes et al., 1998; Bazilevs et al., 2007; Franca et al., 1992). The basis of this stabilization strategy lays in the description of the unknown variables as the sum of a part that can be represented at the scale of finite elements and in a remainder (subgrid scale) that cannot be approximated by finite element shape functions. This stabilization technique is well-assessed in the framework of monophase compressible flows (Koobus and Farhat, 2004; Rispoli and Saavedra, 2006; Bayona Roa et al., 2016), whereas it has been much less used for multi-phase compressible cases (Montanino et al., 2021).

To show the applicability of the proposed formulation to the simulation of pyroclastic gravity currents, we present the solution of well-known benchmark problems for monophase and multiphase flows, showing accuracy and convergent behavior of the method. Furthermore, the impact of pyroclastic flow on an urban settlement is also analyzed considering realistic flow characteristics, material properties, and scale of the problem.

The work is structured as follows: in Section 2 we present the governing equations of the problem and introduce the hypotheses of kinetic and thermal equilibrium; in Section 3 we derive the weak form of the governing equations and introduce the VMS stabilization; in Section 4 we present the application of the method to some benchmark problems, and finally, in Section 5, we draw some conclusions and discuss the future perspectives for this work.

## 2. Governing equations

The flow of a dilute multiphase flow (with solid concentration $\varepsilon_s < 10^{-2}$) is described by the equations of conservation of mass, linear momentum, and total energy of each phase (Pelanti and LeVeque, 2006)

$$\frac{\partial}{\partial t}(\varepsilon_g \rho_g) + \frac{\partial}{\partial x_i}(\varepsilon_g \rho_g u_{g,i}) = 0 \tag{1a}$$

$$\frac{\partial}{\partial t}(\varepsilon_g \rho_g u_{g,i}) + \frac{\partial}{\partial x_j}(\varepsilon_g \rho_g u_{g,i} u_{g,j} + p) = \frac{\partial \tau_{g,ij}}{\partial x_j} + \varepsilon_g \rho_g b_{g,i} - D(u_{g,i} - u_{s,i}) \tag{1b}$$

$$\frac{\partial}{\partial t}(\varepsilon_g\rho_g e_g) + \frac{\partial}{\partial x_i}((\varepsilon_g\rho_g e_g + p)u_{g,i}) = u_{g,i}\frac{\partial}{\partial x_j}\tau_{g,ij} - \frac{\partial}{\partial x_i}q_{g,i} + \varepsilon_g\rho_g b_{g,i}u_{g,i} + \varepsilon_g\rho_g r_g - D(u_{g,i} - u_{s,i})u_{g,i} - Q(T_g - T_s) \tag{1c}$$

$$\frac{\partial}{\partial t}(\varepsilon_s\rho_s) + \frac{\partial}{\partial x_i}(\varepsilon_s\rho_s u_{s,i}) = 0 \tag{1d}$$

$$\frac{\partial}{\partial t}(\varepsilon_s\rho_s u_{s,i}) + \frac{\partial}{\partial x_j}(\varepsilon_s\rho_s u_{s,i}u_{s,j}) = \frac{\partial \tau_{s,ij}}{\partial x_j} + \varepsilon_s\rho_s b_{s,i} + D(u_{g,i} - u_{s,i}) \tag{1e}$$

$$\frac{\partial}{\partial t}(\varepsilon_s\rho_s e_s) + \frac{\partial}{\partial x_i}(\varepsilon_s\rho_s e_s u_{s,i}) = u_{s,i}\frac{\partial}{\partial x_j}\tau_{s,ij} - \frac{\partial}{\partial x_i}q_{s,i} + \varepsilon_s\rho_s b_{s,i}u_{s,i} + \varepsilon_s\rho_s r_s + D(u_{g,i} - u_{s,i})u_{s,i} + Q(T_g - T_s) \tag{1f}$$

where $\varepsilon_g$ and $\varepsilon_s$ are the volumetric fractions of the gas and the solid phases being $\varepsilon_g + \varepsilon_s = 1$, $\rho_g$ and $\rho_s$ are the densities, $\boldsymbol{u}_g$ and $\boldsymbol{u}_s$ are the velocity fields, $e_g$ and $e_s$ are the specific energies, where in particular

$$e_g = c_v T_g + \frac{1}{2}u_{g,i}u_{g,i} \quad \text{and} \quad e_s = c_s T_s + \frac{1}{2}u_{s,i}u_{s,i} \tag{2}$$

where $c_v$ and $c_s$ are the specific heat at constant volume of the gas, and the one of the solid material, respectively, $T_g$ and $T_s$ are the gas and solid temperatures. Moreover, $p = \varepsilon_s p_g$ is the total pressure, being $p_g$ the pressure of the gas phase; $\boldsymbol{b}_g$ and $\boldsymbol{b}_s$ are body forces of the two phases, and $r_g$ and $r_s$ are heat sources. Finally, $\boldsymbol{\tau}_g$ and $\boldsymbol{\tau}_s$ are the stress tensors of each mixture phase, analogously $\boldsymbol{q}_g$ and $\boldsymbol{q}_s$ are the heat flows of each phase. The momentum and energy exchanges between the solid and the gas phases are modeled through the terms $Q(T_g - T_s)$ and $D(\boldsymbol{u}_g - \boldsymbol{u}_s)$, that vanish when the velocity and temperature fields of the two phases are the same.

The formulation is completed by the equations of state. For the gas phase, this reads

$$p_g = \rho_g R T_g \tag{3}$$

being $R$ the specific constant of the gas; for the solid phase, one must simply state the incompressibility of the solid material, *i.e.* $\rho_s = const.$

When a solid particle of radius $\sigma$ and mass $m$ enters in a gas flow with dynamic viscosity $\mu_g$, the difference of velocities between the particle and the flow reduces and tends asymptotically to zero (Marble, 1970). This process is exhausted in a characteristic time

$$\tau_U = \frac{m}{6\pi\sigma\mu_g} \tag{4}$$

A similar phenomenon occurs for the temperature difference, that tends to zero after the following characteristic time

$$\tau_T = \frac{mc_p}{4\pi\sigma\lambda} \tag{5}$$

where $c_p$ is the specific heat of the mixture and $\lambda$ is the thermal diffusivity of the gas phase.

It follows that, after a time $t$ from the volcanic event such that $t > \tau_U$ and $t > \tau_T$ , the temperature and velocity fields of the two phases are uniform, therefore we can set $\boldsymbol{u}_g = \boldsymbol{u}_s = \boldsymbol{u}$, and $T_g = T_s = T$. This condition is known as the hypothesis of thermal and kinetic equilibrium (Cerminara et al., 2016). Using this assumption and summing Equations (1a) and (1d), Equations (1b) and (1e), and Equations (1c) and (1f), we obtain

$$\frac{\partial}{\partial t}\rho + \frac{\partial}{\partial x_i}(\rho u_i) = 0 \tag{6a}$$

$$\frac{\partial}{\partial t}(\rho u_i) + \frac{\partial}{\partial x_j}(\rho u_i u_j + p) = \frac{\partial \tau_{ij}}{\partial x_j} + \rho b_i \tag{6b}$$

$$\frac{\partial}{\partial t}E + \frac{\partial}{\partial x_i}((E+p)u_i) = u_i\frac{\partial}{\partial x_j}\tau_{ij} - \frac{\partial}{\partial x_i}q_i + \rho b_i u_i + \rho r \tag{6c}$$

We also retain Equation (1d) to control the conservation of the solid phase mass, and we rewrite it in terms of the new uniform velocity field as

$$\frac{\partial}{\partial t}(\varepsilon_s\rho_s) + \frac{\partial}{\partial x_i}(\varepsilon_s\rho_s u_i) = 0 \tag{7}$$

In Equation (6) $\rho = \varepsilon_g\rho_g + \varepsilon_s\rho_s$ is the total density of the mixture, and $E = \varepsilon_g\rho_g e_g + \varepsilon_s\rho_s e_s$ is the total mixture energy; the stress tensor and the heat flow vector are written as linear terms with a new mixture viscosity $\mu_m$ and mixture thermal diffusivity $\lambda_m$, following (Marble, 1970), as

$$\mu_m = \frac{\mu_g}{1+\kappa} \qquad \text{and} \qquad \lambda_m = \frac{\lambda_g}{1+\kappa} \tag{8}$$

being $\kappa = \varepsilon_s\rho_s/_g\rho_g$.

## 3. Weak form and stabilization

In this section, we introduce the weak form of Problem (6)-(7). First, for convenience, we reformulate the problem in terms of a set of *conservative* variables as

$$\frac{\partial}{\partial t}U_i + \frac{\partial}{\partial x_j}F_{ij} = \frac{\partial}{\partial x_i}G_{ij} + S_{ij}U_j \tag{9}$$

where $\boldsymbol{U}$ is the vectcor of conservative variables, $\boldsymbol{F}$ and $\boldsymbol{G}$ represent the convective and the dissipative flux, respectively, and $\boldsymbol{S}$ is the matrix of the source terms.

For the case of multiphase flows, the set of conservative variables is

$$\boldsymbol{U} = [\rho, P_s, \boldsymbol{M}, E]^T \tag{10}$$

where $P_s = \varepsilon_s \rho_s$ is the contribution of the solid phase to the total mixture density, and $\boldsymbol{M} = \rho \boldsymbol{u}$ is the total linear momentum of the mixture; consequently, the convective and diffusive fluxes are

$$\mathbf{F} = \begin{bmatrix} M_j \\ \frac{P_s}{\rho} M_j \\ M_i \frac{M_j}{\rho} + p\delta_{ij} \\ \frac{M_j}{\rho}(E + p) \end{bmatrix}, \qquad \mathbf{G} = \begin{bmatrix} 0_j \\ 0_j \\ \tau_{ij} \\ u_i \tau_{ij} + q_j \end{bmatrix} \tag{11}$$

where $i, j$ range from 1 to $d$ being $d$ the space dimensions, and $\delta_{ij}$ is the Kronecker delta. Moreover, the pressure $p$ can be expressed in terms of the conservative variable, using the equation of state and the definition of the total energy.

Finally, the source term matrix is

$$\mathbf{S} = \begin{bmatrix} 0 & 0 & \mathbf{0}^T & 0 \\ 0 & 0 & \mathbf{0}^T & 0 \\ \mathbf{b} & \mathbf{0} & \mathbf{0} & \mathbf{0} \\ r & 0 & \mathbf{b}^T & 0 \end{bmatrix} \tag{12}$$

We obtain the weak form of Equation (9) by pre-multiplying it by a test function vector $\boldsymbol{V}$ and integrating over the domain $\Omega$ as

$$\left(V_i, \frac{\partial}{\partial t} U_i\right) + \left(V_i, A_{ijk} \frac{\partial}{\partial x_j} U_k\right) = \left(V_i, \frac{\partial}{\partial x_j} G_{ij}\right) + (V_i, S_{ij} U_j) \tag{13}$$

which can be rewritten integrating by part the diffusive term, and incorporating the source term into the non linear, convective term

$$\left(V_i, \frac{\partial}{\partial t} U_i\right) + \left(V_i, A_{ijk} \frac{\partial}{\partial x_j} U_k - S_{ij} U_j\right) + \left(\frac{\partial}{\partial x_j} V_i, G_{ij}\right) \tag{14}$$

being

$$A_{ijk} = \frac{\partial F_{ij}}{\partial U_k} \tag{15}$$

the Euler-Jacobian matrix.

A Finite Element discretization of Equation (14) leads to unphysical oscillations of variables, due to the dominance of the convective part. This kind of instability has been the object of diffuse literature (Codina, 2002, 2000) and has been tackled with different approaches. Here, we use the Variational Multiscale (VMS) technique (Hughes et al., 1998) as the stabilizing tool. In the VMS spirit, the vectors of conservative variables and the test function are decomposed into two parts, a first one ($\boldsymbol{U}^h$) that can be represented at the scale of Finite Elements, and the second one ($\tilde{\boldsymbol{U}}$) that is representative of the fluctuations occurring at a finer scale.

$$\boldsymbol{U} = \boldsymbol{U}^h + \tilde{\boldsymbol{U}}\,, \qquad \boldsymbol{V} = \boldsymbol{V}^h + \tilde{\boldsymbol{V}} \tag{16}$$

Following the formulation proposed in (Bayona Roa et al., 2016) for compressible monophase flows, and adapted in (Montanino et al., 2021) for multiphase flows, we discretize the following weak form

$$\left(V_i^h, \frac{\partial U_i}{\partial t} + L_{ik} U_k\right) - \left(L_k^*, \tau_{kj} R_j^h\right) + \left(\frac{\partial V_i^h}{\partial x_j}, G_{ij}(\mathbf{U}_h)\right) = 0 \tag{17}$$

where the second term is the stabilizing part, in accordance to the the prescription of the VMS. In Equation (17)

$$L_k^* = \frac{\partial V_i^h}{\partial x_j} A_{ijk} + V_i B_{ijkm} \frac{\partial U_m^h}{\partial x_j} - V_i S_{ik} \tag{18}$$

is the adjoint term, $\boldsymbol{R}^h$ is the residual of the Finite Element scale, and $\boldsymbol{\tau}$ is the diagonal matrix of the stabilizing terms, being

$$\boldsymbol{\tau}^{-1} = \begin{bmatrix} \tau_\rho^{-1} & 0 & 0 & 0 \\ 0 & \tau_\rho^{-1} & 0 & 0 \\ 0 & 0 & \tau_M^{-1} & 0 \\ 0 & 0 & 0 & \tau_E^{-1} \end{bmatrix} \tag{19}$$

with

$$\tau_\rho^{-1} = c_2 \frac{u + c_m}{h}, \quad \tau_M^{-1} = c_1 \frac{\nu}{h^2} + c_2 \frac{u + c_m}{h}, \quad \tau_E^{-1} = c_1 \frac{\lambda_m}{\rho c_{p.m} h^2} + c_2 \frac{u + c}{h} \tag{20}$$

where $c_1$ and $c_2$ are algorithmic constant, set to $c_1 = 4$ and $c_2 = 2$; $c_m$ is the mixture speed of sound (Pelanti and LeVeque, 2006), $c_p$ is the mixture specific heat at constant pressure (Marble, 1970), and finally $h$ is the characteristic length of the element.

The numerical solution of Equation (17) is got after discretization in space and time. In particular, linear finite elements are used for spatial discretization, and an explicit first-order Euler scheme is used as time integration scheme. For details about the discrete form of the problem we refer to (Montanino et al., 2021).

The overall implementation of the numerical formulation is done in Kratos Multiphysics (Dadvand et al., 2010), an open-source coding environment suited for parallelization using FEM.

## 4. Application

In this section, we apply the formulation developed above to two different cases. First, we analyze the Sod shock tube, a well-known benchmark case for compressible flows, to assess the accuracy of the formulation and discuss its convergent behavior. Then, the method is applied to the case of a pyroclastic current hitting two buildings. This test is approached considering realistic material and geometrical data.

For both cases, the parameters adopted are $\rho_s = 1800$ kg/m$^3$, $c_v = 722$ W/Kg K, $c_p = 1010$ W/Kg K, $c_s = 1300$ W/kg K.

### 4.1. Sod shock tube

The Sod tube is a common benchmark for testing the performances of different numerical methods for monophase compressible flows (Cremonesi and Frangi, 2016; Fu, 2019).

It consists of a two-dimensional rectangular domain with the length ($L = 1$ m) much higher than the height in order to enforce a monodimensional flow. A membrane separates the domain into two parts that are filled with a gas at different initial conditions. In the left part, the gas density is $\rho_g = 1$ kg/m$^3$ and its pressure $p = 1$ Pa, while, in the right side, the gas density is $\rho_g = 0.125$ kg/m$^3$ and its pressure is $p = 0.1$ Pa. The initial velocity for all the domain is $u = 0$ m/s. To reproduce the standard monophase case typically solved in the literature, we assume here that there is no solid concentration in the domain ($\varepsilon_s = 0$). At $t = 0$ s, the membrane is removed, and the jumps in pressure and density between the two parts of the domain give rise to a shock wave propagating toward the right side of the domain, and to a refracting wave moving toward the left side. Both waves move at the speed of sound, which depends on the characteristics of the gas. For the monophase case, the test has an analytical solution that can be obtained through an iterative procedure, such that presented in (Toro, 2013).

The velocity analytical solution at $t = 0.2$ s is represented in Figure 1 together with the numerical solutions obtained for different discretizations. The graph shows a good agreement between the numerical and the analytical solution, and a clear convergence to the analytical solution for reducing mesh sizes.

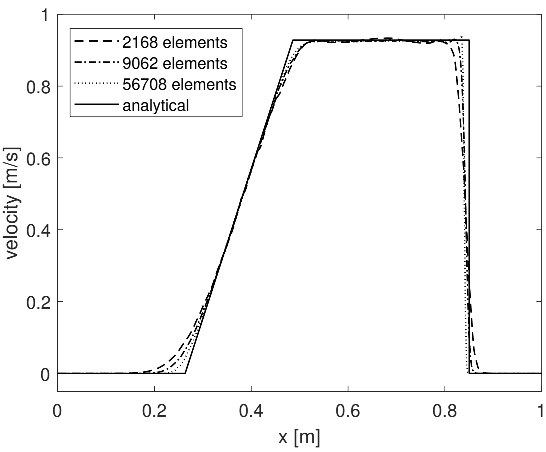


*Figure 1.* Monophase shock tube - velocity distribution at $t = 0.2$ s.

Here, we propose a modification of the standard monophase Sod tube problem to assess the accuracy of the multiphase formulation. In particular, we consider the same values for the gas density $\rho_g$, pressure $p$, and velocity as the monophase case, but we include in all the domain a concentration of solid particles. Three different solid concentrations are considered in three different analyses, namely $\varepsilon_s = 10^{-5}$, $\varepsilon_s = 10^{-4}$, and $\varepsilon_s = 10^{-3}$.

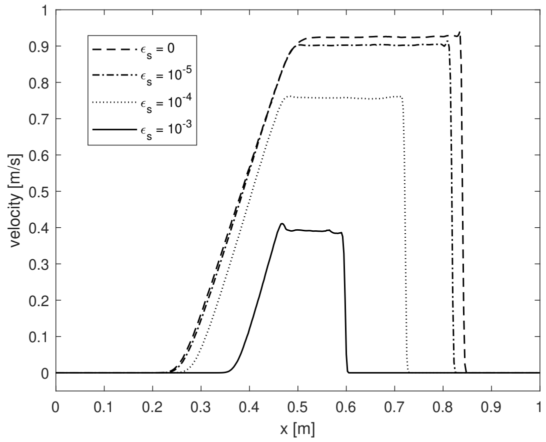


*Figure 2.* Multiphase shock tube - velocity distribution at $t = 0.2$ s.

In Figure 2, we show the velocity distribution over the $x$-axis for the three different cases. For comparison purposes, the monophase case solution obtained with a discretization of 56708 finite elements is also plotted in the same graph.

We observe that both on the left and the right sides, the initial velocity is preserved in a larger zone for increasing values of the solid phase concentration. This is due to the fact that the speed of sound in the mixture is lower than the one of the monophase case.

In Figures 3, we show the convergence of the velocity field at $t = 0.2$ considering different discretizations and the highest solid phase concentrations ($\varepsilon_s = 10^{-4}$ and $\varepsilon_s = 10^{-3}$). Although no analytical solution is known for this case, the convergence of the solution is assessed.

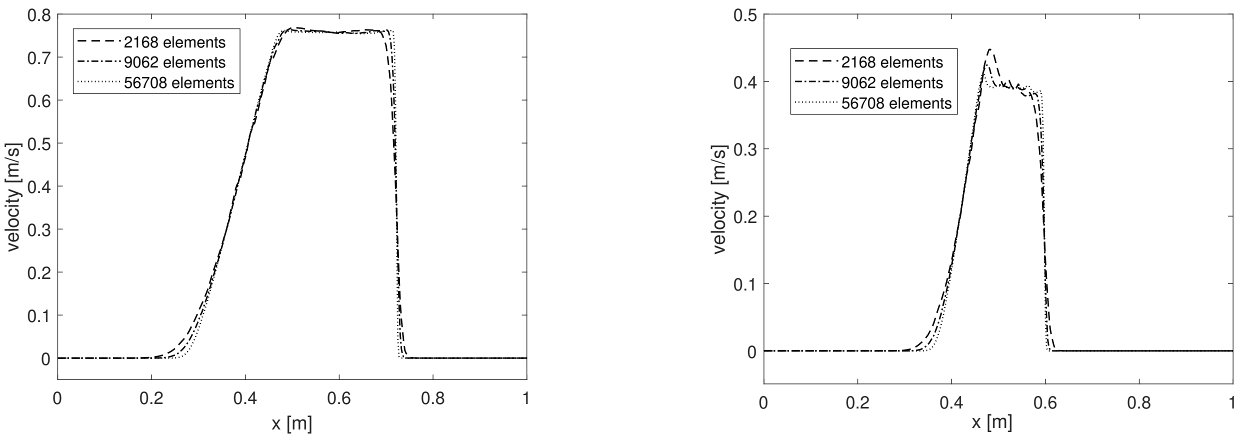


*Figure 3.* Multiphase shock tube - velocity distribution at $t = 0.2$ s for the cases $\varepsilon = 10^{-4}(left)$ and $\varepsilon = 10^{-3}$ (right).

## 4.2. Pyroclastic gravity current

In this section, we consider hypothetical scenarios of a pyroclastic gravity current hitting two buildings. We analyze the phenomena at a distance from the volcanic eruption such that the hypotheses of kinetic and thermal equilibrium can be assumed. For this case, the air viscosity is set to $\mu = 10^{-5}$ kg/m s and the thermal conductivity is $\lambda_g = 0.026$ W/m K.

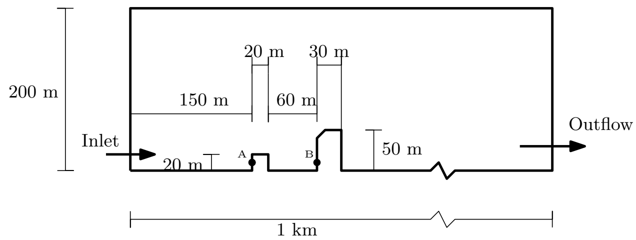


*Figure 4.* Real scale application: Computational domain used for the simulation.

The computational domain is depicted in Figure 4. We assume as initial condition still air at a density $\rho_g = 1.225$ kg/m$^3$ and temperature $T = 300$ K.

Concerning the boundary conditions, the inlet is on the left side of the domain and is described by

$$\begin{cases} \varepsilon_s(x_1 = 0, x_2, t) = \varepsilon_{s,max}\alpha(x_2)\beta(t) \\ u_1(x_1 = 0, x_2, t) = u_{1,max}\alpha(x_2)\beta(t) \\ u_2(x_1 = 0, x_2, t) = 0\,\mathrm{m/s} \\ T(x_1 = 0, x_2, t) = 300\ \mathrm{K} \end{cases} \tag{21}$$

where $\varepsilon_{s,max}$ and $u_{1,max}$ are the maximum values assumed by the solid concentration and of the mixture velocity at the inlet.

The functions $\alpha(x_2)$ and $\beta(t)$ are shown in Figure 5; $\alpha(x_2)$ represents the spatial distribution of the inlet solid concentration and the mixture velocity, and it decreases with the altitude from the ground level; $\beta(t)$ has a periodic behavior and simulates the different waves of pyroclastic material.

We perform two different simulations, considering a solid concentration of $\varepsilon_{s,max} = 5 \cdot 10^{-3}$ in the first case, and $\varepsilon_{s,max} = 1 \cdot 10^{-3}$ in the second case. For both analyses, we consider $u_{1,max} = 60$ m/s.

In Figure 6, we report the results in terms of pressure difference with respect to the atmospheric conditions measured at points A and B. We observe that, as the solid concentration reaches the first building (after about 10 seconds from the beginning of the simulation), for both the cases $\varepsilon_{s,max} = 5 \cdot 10^{-3}$ and $\varepsilon_{s,max} = 1 \cdot 10^{-3}$ the pressure at point $A$ increases with respect to the atmospheric conditions, whereas the point $B$ does not experience any pressure variation. After hitting the first obstacle with a different impact velocity depending on the solid concentration, the pyroclastic current reaches the second building (point $B$) giving rise to an increase of pressure on it. As expected, for higher values of solid concentration, the pressure jump is higher and occurs before.

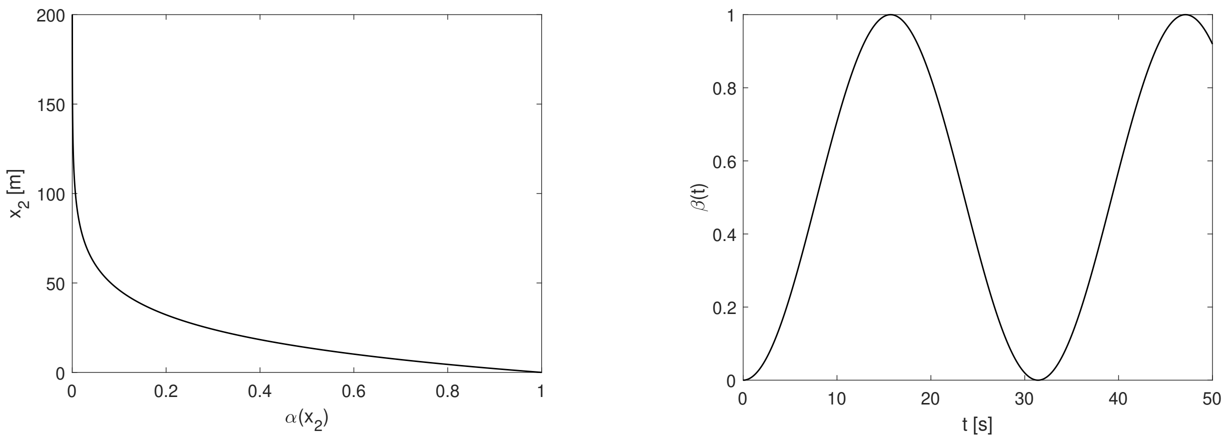


*Figure 5.* Real scale application: function $\alpha(x_2)$ and $\beta(t)$ for the description of the inlet

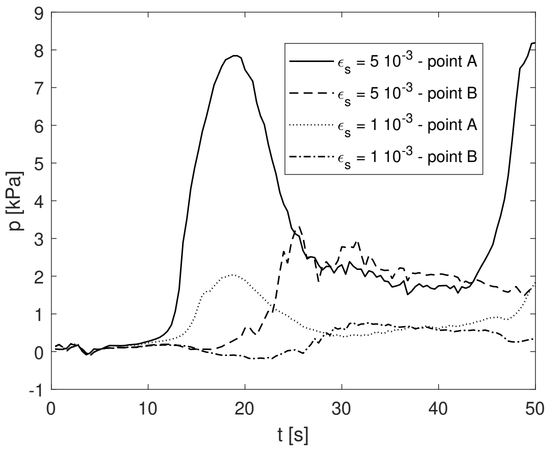


*Figure 6.* Real scale application: pressure at points $A$ and $B$ for two different intensities of solid concentration.

To further analyze the dynamics of the problem, in Figures 7 we show the solid phase concentration distribution at some significant instants of the simulation. In particular, in Figures 7a and 7b ($t = 14$ s), the simulation with $\varepsilon_{s,max} = 5 \cdot 10^{-3}$ reaches the first obstacle, whereas the more diluted one is still far. This is consequence of the minor kinetic energy possessed by the flow with lower solid phase concentration.

Figures 7c and 7d (at $t = 21$ s) show that while the denser flow is already hitting the second building, the other one has just overcome the first building.

Finally, in Figures 7e and 7f (at $t = 28$ s) the denser mixture reaches the ground behind the second building and has already filled the gap between the two buildings, while the more diluted distribution is still collapsing onto the second building.

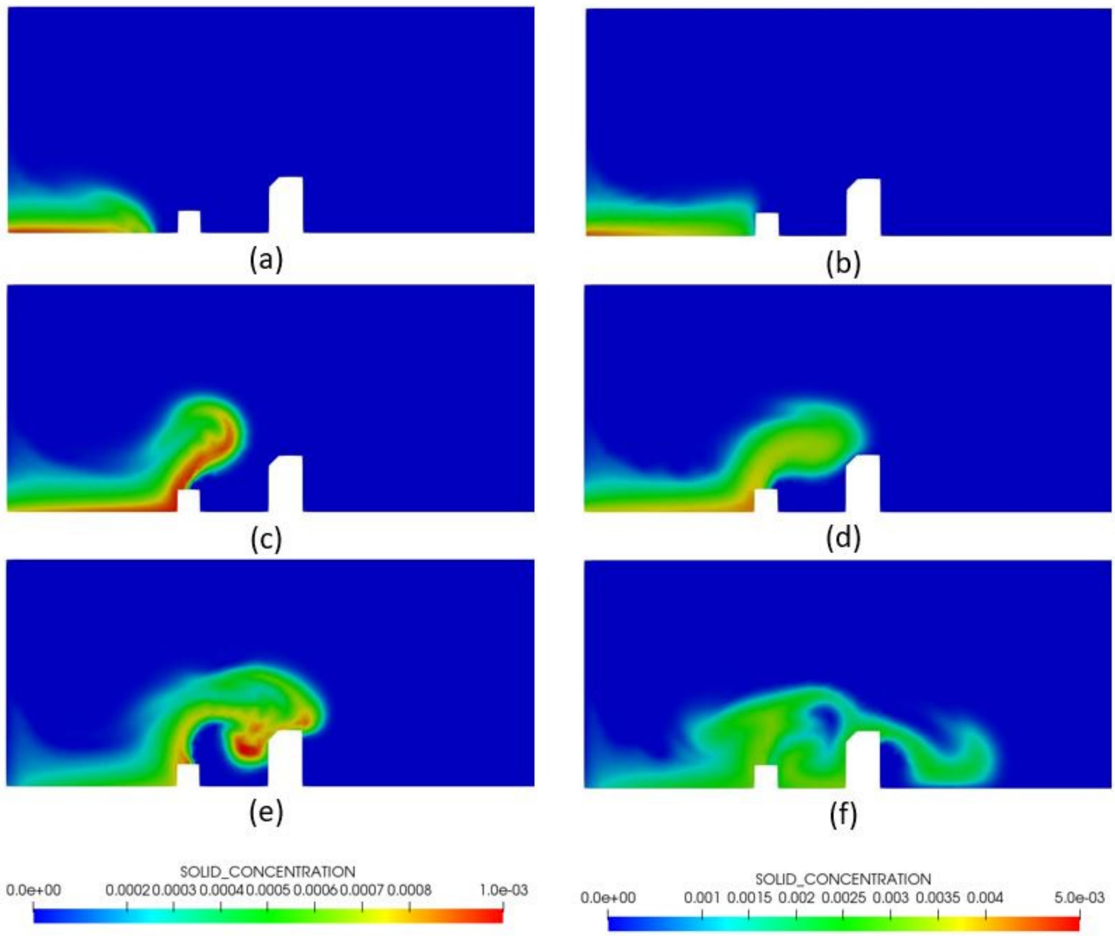


*Figure 7.* Real scale application: solid phase distribution at different instants.
$t = 14$ s: (a) $\varepsilon_{s,max} = 1 \cdot 10^{-3}$; (b) $\varepsilon_{s,max} = 5 \cdot 10^{-3}$;
$t = 21$ s: (c) $\varepsilon_{s,max} = 1 \cdot 10^{-3}$; (d) $\varepsilon_{s,max} = 5 \cdot 10^{-3}$
$t = 28$ s: (e) $\varepsilon_{s,max} = 1 \cdot 10^{-3}$; (f) $\varepsilon_{s,max} = 5 \cdot 10^{-3}$

The proposed simulation, with realistic values for the geometry of a urban settlement and for the gas and solid properties, is able to describe effectively the barrier effect that occurs between buildings during a pyroclastic event, showing the reduced values of the pressure on building less exposed to the the mixture current.

## 5. Conclusion

In this work, we have presented a stabilized finite element formulation for the description of pyroclastic gravity currents generated by explosive volcanic eruptions. In particular, we adopted a

Variational Multiscale Method, recently extended to multiphase compressible flows, to stabilize the finite element formulation and thus to avoid spurious oscillations of the solution variables.

The formulation is here tested and assessed against well-known benchmarks for compressible flow problems and applied to a real scale application considering a pyroclastic current hitting some buildings.

In all examples, the developed finite element formulation has shown robustness, convergence and accuracy, and it has demonstrated its potential for the evaluation of the effects of volcanic hazard on civil constructions placed at a certain distance from the volcano.

Future developments of this work foresee parametric analyses to assess the influence of different geometrical and physical quantities on the quantification of the hazard, as well as the extension to three-dimensional cases and the application to the real topography of the urban agglomerates around the Vesuvius volcano.

## References

Baxter, P. J., Boyle, R., Cole, P., Neri, A., Spence, R., and Zuccaro, G. (2005). The impacts of pyroclastic surges on buildings at the eruption of the soufrière hills volcano, montserrat. *Bulletin of volcanology*, 67(4):292–313.

Bayona Roa, C. A., Baiges, J., and Codina, R. (2016). Variational multi-scale finite element approximation of the compressible navier-stokes equations. *International Journal of Numerical Methods for Heat & Fluid Flow*.

Bazilevs, Y., Calo, V., Cottrell, J., Hughes, T., Reali, A., and Scovazzi, G. (2007). Variational multiscale residual-based turbulence modeling for large eddy simulation of incompressible flows. *Computer methods in applied mechanics and engineering*, 197(1-4):173–201.

Bochev, P. B., Gunzburger, M. D., and Shadid, J. N. (2004). Stability of the supg finite element method for transient advection–diffusion problems. *Computer methods in applied mechanics and engineering*, 193(23-26):2301–2323.

Cerminara, M., Esposti Ongaro, T., and Berselli, L. C. (2016). Ashee-1.0: a compressible, equilibrium–eulerian model for volcanic ash plumes. *Geoscientific Model Development*, 9(2):697–730.

Codina, R. (2000). Stabilization of incompressibility and convection through orthogonal sub-scales in finite element methods. *Computer methods in applied mechanics and engineering*, 190(13-14):1579–1599.

Codina, R. (2002). Stabilized finite element approximation of transient incompressible flows using orthogonal subscales. *Computer methods in applied mechanics and engineering*, 191(39-40):4295–4321.

Cremonesi, M. and Frangi, A. (2016). A lagrangian finite element method for 3d compressible flow applications. *Computer Methods in Applied Mechanics and Engineering*, 311:374–392.

Dadvand, P., Rossi, R., and Oñate, E. (2010). An object-oriented environment for developing finite element codes for multi-disciplinary applications. *Archives of computational methods in engineering*, 17(3):253–297.

Esposti Ongaro, T., Cavazzoni, C., Erbacci, G., Neri, A., and Salvetti, M.-V. (2007). A parallel multiphase flow code for the 3d simulation of explosive volcanic eruptions. *Parallel Computing*, 33(7-8):541–560.

Franca, L. P., Frey, S. L., and Hughes, T. J. (1992). Stabilized finite element methods: I. application to the advective-diffusive model. *Computer Methods in Applied Mechanics and Engineering*, 95(2):253–276.

Fu, L. (2019). A low-dissipation finite-volume method based on a new teno shock-capturing scheme. *Computer Physics Communications*, 235:25–39.

Hughes, T. J., Feijóo, G. R., Mazzei, L., and Quincy, J.-B. (1998). The variational multiscale method—a paradigm for computational mechanics. *Computer methods in applied mechanics and engineering*, 166(1-2):3–24.

Iacuaniello, M., Montanino, A., De Gregorio, D., and Zuccaro, G. (2020). Pyroclastic flow mitigation strategies: a new perspective for the red area. *Natural Hazards and Earth System Sciences Discussions*, pages 1–28.

Koobus, B. and Farhat, C. (2004). A variational multiscale method for the large eddy simulation of compressible turbulent flows on unstructured meshes—-application to vortex shedding. *Computer Methods in Applied Mechanics and Engineering*, 193(15-16):1367–1383.

Marble, F. E. (1970). Dynamics of dusty gases. *Annual Review of Fluid Mechanics*, 2(1):397–446.

Montanino, A., Franci, A., Rossi, R., and Zuccaro, G. (2021). Finite element formulation for compressible multiphase flows and its application to pyroclastic gravity currents. *submitted to Computational Mechanics*.

Neri, A., Esposti Ongaro, T., Macedonio, G., and Gidaspow, D. (2003). Multiparticle simulation of collapsing volcanic columns and pyroclastic flow. *Journal of Geophysical Research: Solid Earth*, 108(B4).

Pelanti, M. and LeVeque, R. J. (2006). High-resolution finite volume methods for dusty gas jets and plumes. *SIAM Journal on Scientific Computing*, 28(4):1335–1360.

Rispoli, F. and Saavedra, G. R. (2006). A stabilized finite element method based on sgs models for compressible flows. *Computer methods in applied mechanics and engineering*, 196(1-3):652–664.

Tezduyar, T. and Sathe, S. (2003). Stabilization parameters in supg and pspg formulations. *Journal of computational and applied mechanics*, 4(1):71–88.

Toro, E. F. (2013). *Riemann solvers and numerical methods for fluid dynamics: a practical introduction*. Springer Science & Business Media.

Zuccaro, G., Cacace, F., Spence, R., and Baxter, P. (2008). Impact of explosive eruption scenarios at vesuvius. *Journal of Volcanology and Geothermal Research*, 178(3):416–453.

Zuccaro, G. and De Gregorio, D. (2019). Impact assessments in volcanic areas-the vesuvius and campi flegrei cases studies. *Annals of Geophysics*, 62(1):02.

Zuccaro, G. and Leone, M. F. (2012). Building technologies for the mitigation of volcanic risk: Vesuvius and campi flegrei. *Natural hazards review*, 13(3):221–232.